

Article

Construction and Verification of Spherical Thin Shell Model for Revealing Walnut Shell Crack Initiation and Expansion Mechanism

Xiulan Bao ^{1,2}, Biyu Chen ^{1,2}, Peng Dai ^{1,2}, Yishu Li ^{1,2} and Jincheng Mao ^{3,*}¹ College of Engineering, Huazhong Agricultural University, Wuhan 430070, China² Key Laboratory of Agricultural Equipment in Mid-Lower Yangtze River, Wuhan 430070, China³ School of Mechanical and Electrical Engineering, Wuhan Institute of Technology, Wuhan 430073, China

* Correspondence: jun-lan@163.com; Tel.: +86-138-7122-9154

Abstract: Walnut shell breaking is the first step of deep walnut processing. This study aims to investigate the mechanical properties and fracture state of the Qingxiang walnut shell under unidirectional load and guide the complete separation of the walnut shell and kernel. The spherical thin shell model of the walnut (the fitting error is less than 5%) was established and verified. The process from the initiation to the expansion of walnut cracks was analyzed. The crack expansion rate was estimated in terms of the crack fracture regularity on the shell's surface. Based on the momentless theory and finite element simulation analysis, we found that the stress on the shell surface in the concentrated force action region was gradient distributed from inside to outside and that the internal forces were equal in all directions in the peripheral force action region. The unidirectional impact shell-breaking experiments confirmed the reliability of our spherical thin shell model and verified our hypothesis of walnut shell fracture along the longitudinal grain. Our results can provide a theoretical basis for the development and structural optimization of shell-breaking machinery.

Keywords: walnut; physical properties; crack; broken shell experiment



Citation: Bao, X.; Chen, B.; Dai, P.; Li, Y.; Mao, J. Construction and Verification of Spherical Thin Shell Model for Revealing Walnut Shell Crack Initiation and Expansion Mechanism. *Agriculture* **2022**, *12*, 1446. <https://doi.org/10.3390/agriculture12091446>

Academic Editor: Bengang Wu

Received: 17 June 2022

Accepted: 2 September 2022

Published: 13 September 2022

Publisher's Note: MDPI stays neutral with regard to jurisdictional claims in published maps and institutional affiliations.



Copyright: © 2022 by the authors. Licensee MDPI, Basel, Switzerland. This article is an open access article distributed under the terms and conditions of the Creative Commons Attribution (CC BY) license (<https://creativecommons.org/licenses/by/4.0/>).

1. Introduction

Walnut is a plant of the genus *Juglans*, and walnut, cashew, almond, and hazelnut are known as the world's four dried fruit. Walnut kernels are rich in nutrients such as protein, vitamins, and cellulose. It contains high contents of unsaturated fatty acids and multiple proteins, which is very beneficial for health and can strengthen the brain [1–3]. The shell weight of dried fruits such as walnuts is relatively large in proportion to their total weight, but their edible part is little. Moreover, the hard shell poses a serious obstacle to the extraction of effective components (pulp) in processing. Walnut shell, mainly composed of lignin and hemicellulose, is hard with an irregular appearance, and thus it is difficult to peel [4]. Moreover, there is a large difference in size between different walnuts and a complex diaphragm connection between the shell and kernel with a small shell–kernel gap. These factors make it difficult for the walnut shell to be completely separated from the kernel, and thus it is also difficult to achieve a high complete kernel rate.

At present, the manual shell breaking method with a high cost and low efficiency is gradually being replaced by high-efficiency mechanical shell breaking. In order to realize the mechanization of walnut shell breaking, a large number of studies have been conducted [5]. Appropriate moisture content and force loading direction have been reported to greatly improve the processing efficiency and quality of walnuts [6–9]. A large number of tests have revealed that two pairs of normal concentrated forces can better achieve uniform shell rupture [10]. The research on the mechanical properties of walnut shell breaking from the perspective of finite elements provides a theoretical basis for the development of walnut shell breaking machinery [11,12]. Ojolo et al. designed a rotary sheller, but the

shelling effect was far from satisfactory due to the large individual difference in walnut shells [13]. Li et al. developed a cone-basket walnut shell breaking device with a desirable processing effect but relatively low shelling efficiency [14]. Liu et al. designed a flexible belt-shearing extrusion shell-breaking device that improved the shelling rate and reduced the kernel breaking rate [15]. Ding et al. proposed a bionic knocking shell breaking method and developed a bionic knocking walnut shell breaking machine, which exhibited high shell breaking efficiency but a low complete kernel rate [16].

In order to improve the shell breaking efficiency and shell kernel separation rate, this study explored the shell breaking state and mechanical properties of walnut shells under unidirectional load based on the physical characteristics of the walnut shell. The walnut shell is a spherical shell composed of two hemispherical shells that are combined at the suture line (ridge line). It has been reported that when the walnut suture line (ridge line) is loaded with forces, the walnut shell and kernel will be divided into two parts directly from the ridge line. Therefore, this study selected the shell surface except for the ridge line for modeling and investigated the related characteristics of the continuous shell surface to provide a theoretical basis for the development of shell-breaking machinery.

2. Analysis and Verification of Walnut Characteristics

2.1. Materials and Instruments

This study used Qingxiang thin-skinned walnuts as experiment materials. Three sizes of walnuts with a diameter of 35 ± 2 mm for large, 33 ± 2 mm for medium, and 27 ± 2 mm for small were selected as the walnut samples. The test instruments mainly include a texture meter, a digital vernier caliper (with an accuracy of 0.02 mm), and a digital thickness measuring instrument (with an accuracy of 0.02 mm).

2.2. Tests and Analysis

2.2.1. Sphericity Measurement

The measurement direction of the triaxial size of a walnut is shown in Figure 1. The walnut was fixed with a plane fixture, and the maximum measurement value in each direction was used as the measurement result. The three-axis dimensions of three sizes (large, medium, and small) of walnuts were measured by a digital vernier caliper. The measurement results were recorded, and the sphericity was calculated according to Equation (1).

$$S = \frac{\sqrt[3]{abc}}{d} (d = \max\{abc\}) \quad (1)$$

where S is the sphericity, a is the edge diameter (mm), b is the transverse diameter (mm), and c is the longitudinal diameter (mm).

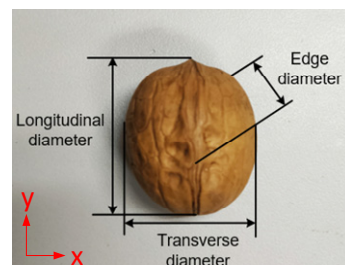


Figure 1. Schematic diagram of walnut diameter.

2.2.2. Sphericity Analysis

The average sphericity of large, medium, and small walnuts was 0.889, 0.883, and 0.904, with the standard deviations of 0.028, 0.012, and 0.019, respectively. Since the sphericity of the walnuts in all three sizes was above 88%, with a very small standard deviation, the selected walnuts were appropriate for approximate spherical modeling.

2.2.3. Shell Thickness Measurement

Since the walnut shell is symmetrically distributed, seven points were selected from half of the shell surface to measure the shell thickness, as shown in Figure 2. The thickness of each sampling point was measured by a digital thickness measuring instrument. Walnuts were divided into three groups (large, medium, and small sizes), with seven walnuts per group and seven thickness measurement points per walnut. The multiple measurement results were averaged.

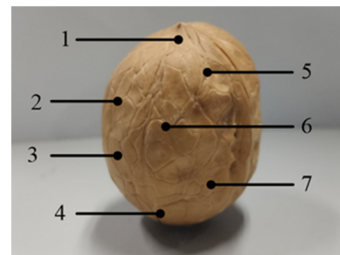


Figure 2. Schematic diagram thickness measurement points of the walnut shell. 1–7 are seven thickness measurement points.

2.2.4. Shell Thickness Analysis

The measurement results of walnut shell thickness at different measurement points are shown in Figure 3. Figure 3 shows that the shell thickness was correlated with the size and measurement point of the walnut. Therefore, these two factors affecting the shell thickness were selected as factor A (walnut size) and factor B (measurement point). Two-Way ANOVA was performed to reveal the difference in shell thickness between different groups (Table 1). The results showed that the p (test value) of the two factors was above 0.01, indicating that the shell thickness at any point on the selected shell surface was uniform between different size groups.

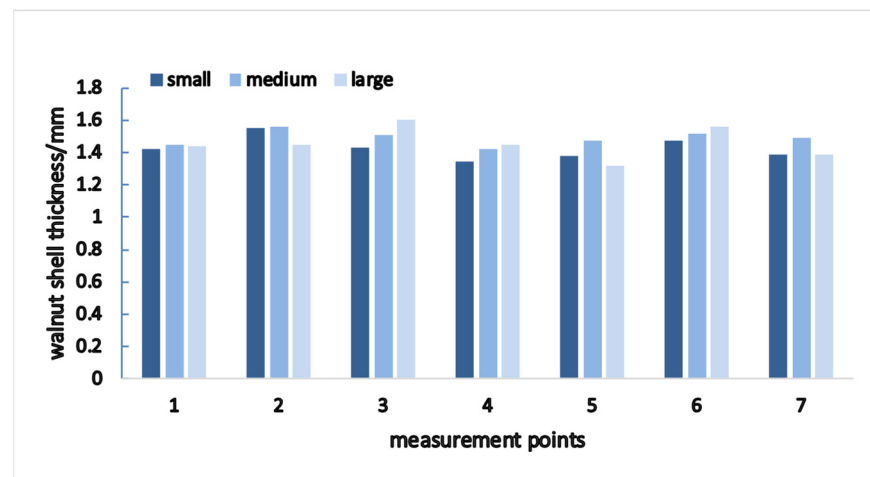


Figure 3. Walnut shell thickness at different measurement points.

Table 1. Two-way ANOVA of shell thickness.

Factors	Sum of Squares	Degree of Freedom	Mean Square	F	p
Factor A	0.01384	2	0.00692	3.89	0.15
Factor B	0.05885	6	0.00981	2.99	0.04
Error	0.03710	12	0.00309		
Sum	0.10978	20			

The above measurement results showed that the walnut shell was approximately spherical and that the shell thickness was uniform. Therefore, the walnut shell was simplified as a spherical thin shell model in this study, and the shell analysis was carried out by establishing the spherical thin shell model.

2.3. Fit Verification of Spherical Thin Shell Model

The previous study has shown that when the load is applied to the walnut, the stress is the largest at the load point, and the deformation area is concentrated near the load point. In addition, the shell thickness and compression stiffness vary with different positions, suggesting the mechanical properties are different at different positions of the walnut shell. When an external load is increased to a certain value, the walnut shell will be unstable or even break. According to elastic mechanics, the critical buckling pressure P_{cr} of thin spherical shells is calculated according to Equation (2):

$$P_{cr} = \frac{2E}{\sqrt{3(1-\mu^2)}} \left(\frac{h}{r}\right)^2 \quad (2)$$

where P_{cr} is the critical pressure (GPa), E is the elastic modulus (GPa), μ is Poisson's ratio, h is the shell thickness (mm), and r is the radius (mm).

Experimental measurements were performed using a texture analyzer. The results were as follows: walnut elastic modulus $E = 0.18$ GPa and Poisson's ratio $\mu = 0.38$. The shell thickness, the radius measurement value ($r = \min\{a, b, c\}/2$), the elastic modulus, and the Poisson's ratio were substituted into the above formula to calculate the critical stress for breaking the shell, and then the shell breaking force was calculated according to the formula $F = P_{cr} \times S$, where F is the shell breaking force, P_{cr} is the critical pressure, S is the compressed area ($S = 100 \text{ mm}^2$), and the corresponding theoretical calculation values are presented in Table 2.

Table 2. Shell breaking force comparison.

Shell-Breaking Force	Sizes		
	Small (27 ± 2 mm)	Medium (33 ± 2 mm)	Large (35 ± 2 mm)
Calculated Value/N	317.3	303.7	312.7
Observed Value/N	329.6	316.1	329.2
Deviation/%	3.7	3.9	5.0

The average shell breaking force of walnut actually measured by the texture analyzer was used as the observed value. The deviation value was calculated by the observed value and the calculated value, with the results presented in Table 2.

As shown in Table 2, there was a certain deviation between the calculated values from the spherical thin-shell model and the actually observed values in this study, indicating that the actual shell shape, shell thickness distribution, and other factors had a certain influence on the force characteristics of walnuts. Since the deviation values in the three groups were less than 5%, a high approximation level and a good model fitting degree were indicated.

3. Crack Analysis

During the experiment, under unidirectional (Y-direction) load, the force was increased with the increase in the downward loading displacement. After reaching the strength limit, the walnut was unstable and fractured. In this process, the fracture first occurred at the maximum stress (the load point). When the downward load displacement continued to increase, the walnut shell continued to bend downward in the load direction. At the same time, the crack expanded outward from the load point and ended when the crack length reached the maximum (Figure 4).



Figure 4. Walnut crack.

3.1. Crack Type

According to the characteristics of force and displacement, cracks fall into three basic types, namely, type I, type II, and type III. In the load concentration area, the load is the normal stress σ , and the direction is perpendicular to the surface of the walnut shell. When it is pressed downward, the walnut will eventually rupture to form a crack, and the relative slippage of a crack occurs between the two surfaces, which is a type II crack. Outside the concentrated action domain, the crack mainly extends outward under the action of the partial force pointing to each side of the walnut, and the crack characterized by tearing from the middle is a type I crack.

3.2. Crack Initiation

According to material mechanics, the brittle material will fail when the maximum principal normal stress reaches the unidirectional strength limit of the material under tensile or compressive load, which is the maximum normal stress yield criterion. The maximum normal stress yield criterion can be specified by the function as follows:

$$\sigma_M = \text{MAX}(|\sigma_x|, |\sigma_y|, |\sigma_z|) \quad (3)$$

where σ_M is the ultimate strength, and σ_x , σ_y , and σ_z are the stresses in the three principal axis directions.

When $\sigma_M < \sigma_u$, the material will not break, and when $\sigma_M \geq \sigma_M$, the material will break. In our walnut shell breaking model, $\sigma_x = 0$, $\sigma_y = P_{cr}$, and $\sigma_z = 0$, and thus the limit pressure strength $\sigma_u = |\sigma_y| = P_{cr}$. Under load P_{cr} , $\sigma_1 = 0$, $\sigma_2 = -p$ (negative sign indicates pressure stress), $\sigma_3 = 0$, as a result, $\sigma_M = |\sigma_2| = p$. When $p \geq P_{cr}$, that is, $\sigma_M \geq \sigma_u$, according to the maximum normal stress yield criterion, the failure fracture of the walnut shell occurred, and the initial crack was generated, which was the crack initiation process.

3.3. Crack Expansion

Generally, two parameters in linear elastic fracture mechanics are employed to measure the crack generation ability, namely energy release rate G and stress intensity factor K . When the energy release rate G or the stress intensity factor K exceeds their critical value ($G \geq G_C$ or $K \geq K_C$), it is considered that fracture occurs, which is the fracture criterion. According to fracture mechanics, stress intensity factor K is a measure of crack severity, which is related to crack size, stress, and geometric shape. This study assumes that the mechanical behavior of a walnut shell is linear elastic, and thus we analyzed the crack characteristics of a walnut shell based on the knowledge of linear elastic fracture mechanics.

One previous study has shown that cracks generated on a certain material tend to expand to the positions where toughness was increasingly lowered. For wood, the toughness along the grain direction is lower than that in other directions, and thus wood tends to fracture in the grain direction [17]. The walnut shells in this study also exhibited a similar breaking pattern, namely, walnut shells fracture in the longitudinal direction (Y -axis direction), which was defined as the “along-grain direction”, and the transverse direction (X -axis direction) is the “horizontal direction”.

Based on this, we hypothesized that walnut shells might fracture “along the longitudinal grain”. To test our hypothesis, the material critical strength K_C was calculated. The stress intensity factor K is related to the applied stress and the crack length. Based on linear elastic fracture mechanics, K is usually calculated by Equation (4) [18]:

$$K = FS\sqrt{\pi a} \quad (4)$$

where parameter F is a function of the ratio a/b , which is related to the geometry; S is the load stress, and a is the crack length.

In the case of the ratio of $\alpha = a/b < 0.4$, F is calculated according to Equation (5):

$$F = 1.12S\sqrt{\pi a} \quad (5)$$

In other cases, where $\alpha = a/b$, F is calculated according to Equation (6):

$$F = \sqrt{\frac{2}{\pi\alpha} \tan \frac{\pi\alpha}{2} \left[\frac{0.923 + 0.199(1 - \sin \frac{\pi\alpha}{2})^2}{\cos \frac{\pi\alpha}{2}} \right]} \quad (6)$$

3.3.1. Longitudinal (Along Grain) Direction

The crack length measurement in the longitudinal direction is shown in Figure 5. When the longitudinal ratio $\alpha = a/b = 0.51$ is substituted into Equation (6), longitudinal $F_Z = 1.48$ (Figure 5). Our results also showed that the average crack length of the longitudinal shell breaking of a walnut shell is $a = 34.3$ mm, and the shell breaking force is $S_Z = 310$ N. When these data were substituted into Equation (4), the fracture toughness along the grain direction of a walnut shell is $K_{ZC} = 1.51$ MPa·m^{1/2}.

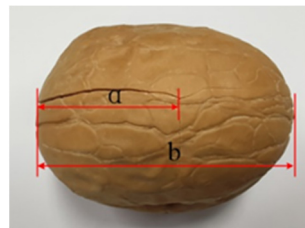


Figure 5. Crack length measurement in the longitudinal direction, a is the crack length, b is the longitudinal diameter.

3.3.2. Horizontal (X-Axis) Direction

The crack length measurement in the transverse direction is shown in Figure 6. When the transverse ratio $\alpha = a/b = 0.50$ was substituted into Equation (6), longitudinal $F_X = 1.47$. In addition, our results showed that the average crack length of a walnut shell is $a = 20.1$ mm, and the shell breaking force is $S_X = 468$ N. When the above data were substituted into Equation (4), we obtained the transverse fracture toughness of a walnut shell as $K_{XC} = 1.72$ MPa·m^{1/2}.

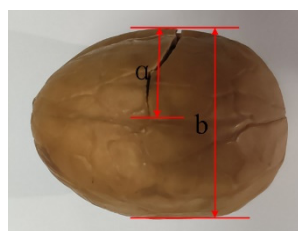


Figure 6. Crack length measurement in the horizontal direction, a is the crack length, b is the transverse diameter.

Our calculation results showed that the transverse fracture toughness was greater than the longitudinal fracture toughness, indicating that the longitudinal intensity is smaller than the transverse intensity, thus confirming our hypothesis that walnut shells might fracture “along longitudinal grain”.

The actual observation also showed that most of the cracks were also longitudinal cracks. Therefore, it can be concluded that no matter whether the initial cracks of walnuts are along the longitudinal direction, they are always affected by the fracture properties along the longitudinal grain during the crack extension process, and under this influence, the cracks would be longitudinally shifted.

3.4. Crack Expansion Rate

In the experiments, the cracking time of a walnut shell under load pressure is so short that the process cannot be observed by eyes. The cracking time of a walnut shell can be estimated according to the relevant formula. According to brittle solid fracture mechanics, the crack expansion rate is calculated by Equation (7) [19]:

$$v(c) = v_T f(c/c_0, \alpha) \quad (7)$$

where v_T is the limit speed, and f is the function of scale one, which is calculated as:

$$f(c/c_0, 0) = 1 - c_0/c \quad (8)$$

where c_0 is the initial crack length, and c is the crack extension length.

The estimation of the limit speed is as follows:

$$v_T \approx 0.38v_1 \quad (9)$$

where $v_1 = (E/\rho)^{1/2}$ is the longitudinal sound rate.

The initial conditions for calculating the crack expansion rate of walnuts are shown in Table 3, and the calculation results are shown in Table 4. The average shell cracking time was calculated as $t = a/v(c) = 4.75 \mu\text{s}$. The calculation results of the crack expansion rate showed that the crack formation time was very short. Based on it, we proposed that it is not necessary to consider the crack formation time. Instead, only the force loading time on the walnut shell surface should be taken into account in practical applications.

Table 3. The initial conditions for calculating the crack expansion rate of walnuts.

Initial Conditions	Elastic Modulus E	Density ρ	Initial Crack Length c_0	Average Length of Cracks a
Initial Value	0.18 GPa	0.5 kg/m ³	0	34.3 mm

Table 4. The calculation results of the walnut crack expansion rate.

Type	The Longitudinal Sound Rate v_1	The Limit Speed v_T	f	The Crack Expansion Rate $v(c)$
Results	19 km/s	7.22 km/s	1	34.3 mm

4. Shell Mechanics Analysis

4.1. Shell Deformation Process

The walnut shell breaking tests under unidirectional load were performed using a texture meter. The force-displacement curve during walnut shell breaking is shown in Figure 7. The force-displacement curve showed that the walnut shell breaking process under force load was summarized as follows: the AB section curve had a small slope with small fluctuations, which might be mainly due to the texture meter cylindrical indenter getting close contact with the irregular surface of the walnut; the BC section was a straight line

with a fixed slope k . According to engineering mechanics, $\sigma = E\varepsilon$. The elastic deformation stage is characterized by a linear relationship between the load and the strain. Therefore, the walnut produces elastic deformation under a load of this section, and thus the BC section was the elastic compression stage. The slope of the CD section was decreased with the increase in the force-displacement in the transverse coordinate compared with that of the BC section. According to material mechanics, the CD section produces not only elastic deformation but also partial plastic deformation, and thus the CD section was a mixed deformation stage of elastic deformation and plastic deformation. When the load was increased to σ_D , the load stress reached the intensity limit of the walnut shell, and thus brittle fracture, as one type of fracture failure, occurred. The EF section showed the stage when the indenter continued to compress the walnut downward. Due to the brittle fracture of the walnut, the toughness of the walnut was reduced to a low value, and thus the load increase under unit displacement was small, eventually resulting in a small slope k . After point F, the texture meter indenter moved back to the initial position, and the load gradually decreased to zero.

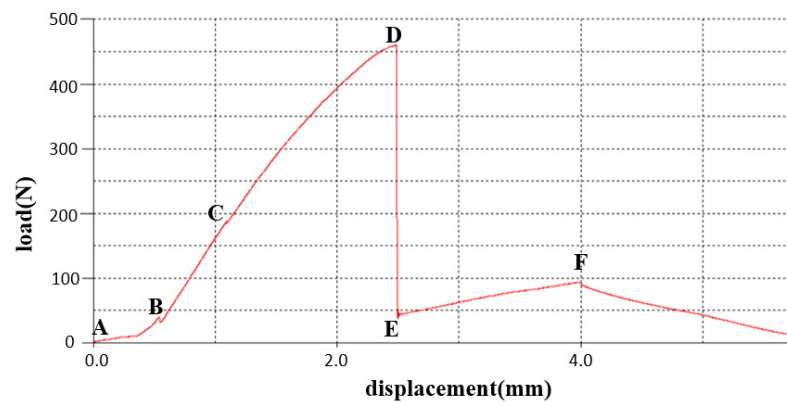


Figure 7. Force—displacement curve of the walnut shell breaking under load.

4.2. Internal Force Analysis

The small thickness and bending moment of the thin shell cause great stress and deformation, which has an important influence on the establishment of the mechanical model. Therefore, this study took the bending moment into full consideration in the analysis of the thin-shell model. In this study, the walnut shell was divided into the concentrated force region and peripheral force region. The concentrated force region was the region undertaking the unidirectional load. The presence of the normal external load resulted in a large bending moment in this region, which could not be ignored. Excluding the concentrated force region, the remaining region far from the concentrated force was defined as the peripheral force region with a negligible small bending moment.

4.2.1. Peripheral Force Region

Since the bending moment in the peripheral force region was negligible, the thin film theory (namely, the momentless theory) could be used for analysis. In a momentless state (Figure 8), only the stresses T_θ , T_φ , and $T_{\theta\varphi}$ were examined, while torques M_θ , M_φ , and $M_{\theta\varphi}$ were ignored. In equilibrium state:

$$M_\theta = M_\varphi = M_{\theta\varphi} = N_\theta = N_\varphi = 0 \quad (10)$$

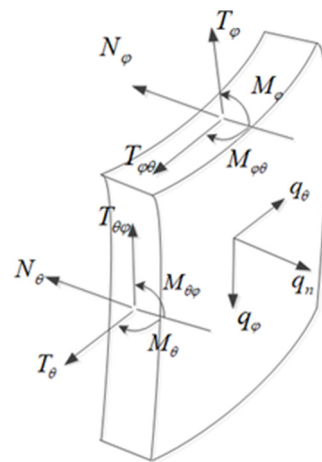


Figure 8. Section diagram of force.

Under static balance conditions:

$$T_\phi r_0 \sin \phi = - \int_0^\phi r_0 R (q_\phi \sin \phi - q_n \cos \phi) d\phi \tag{11}$$

In any cross-section of the walnut shell (Figure 9), $q_\phi = 0, q_n = -p, R = r, r_0 = r \sin \phi$.

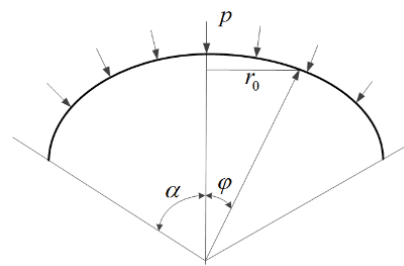


Figure 9. Cross-section diagram of force.

Thus:

$$T_\phi r \sin^2 \phi = - \int_0^\phi r^2 \sin \phi p \cos \phi d\phi \tag{12}$$

Thus:

$$T_\phi = - \frac{pr}{2} \tag{13}$$

Then, by the formula:

$$\frac{T_\phi}{R_1} + \frac{T_\theta}{R_2} - q_n = 0 \tag{14}$$

where R_1 and R_2 are the radiuses of the primary curvature, $R_1 = R_2 = r$, thus:

$$T_\theta = - \frac{pr}{2} \tag{15}$$

The results showed that T_θ was equal to T_ϕ , and thus the internal force was equal in any cross-section of the walnut shell surface within the peripheral force region, indicating that the peripheral force region of the walnut shell had an isotropic property.

4.2.2. Concentrated Force Action Region

The external load in the concentrated force action region resulted in a large unignorable bending moment. Therefore, this region cannot be simply analyzed by the momentless theory, and we resorted to the corresponding moment theory for mechanical analysis. In this study, the finite element analysis method was employed to simulate the concentrated force

action area of the walnut shell to obtain an intuitive and specific shell stress distribution pattern. To this end, the walnut model was constructed, and the concentrated force was analyzed as follows.

Modeling: A 3D walnut model was constructed using a 3D scanner, and then the obtained 3D model was introduced into the finite element software ANSYS (Figure 10).

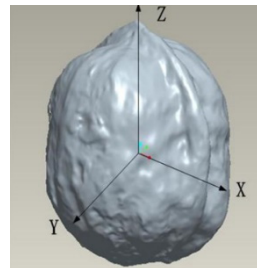


Figure 10. Walnut 3D scanned model.

Parameter setting: The elastic modulus of the walnut model was set as 0.18 GPa, the Poisson ratio as 0.3, and the walnut shell density as 0.5 kg/m^3 .

Meshing: The grid properties were set, and the grid was endowed with material properties. The model was meshed with a mesh quality of >0.3 , indicating a suitable meshing (Figure 11).

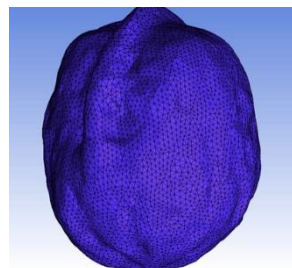


Figure 11. Meshing of the walnut model.

Force analysis: The 100 N contact load was added to the model, and then the simulation analysis of the loaded model was performed. The stress cloud diagram was obtained from the simulation analysis (Figure 12). The stress cloud diagram intuitively reflected the stress distribution in the concentrated force region. The results showed that under the load, the shell stress was gradient-distributed along the walnut shell, reaching the maximum at the load point, and it gradually decreased with the increasing distance from the load point.

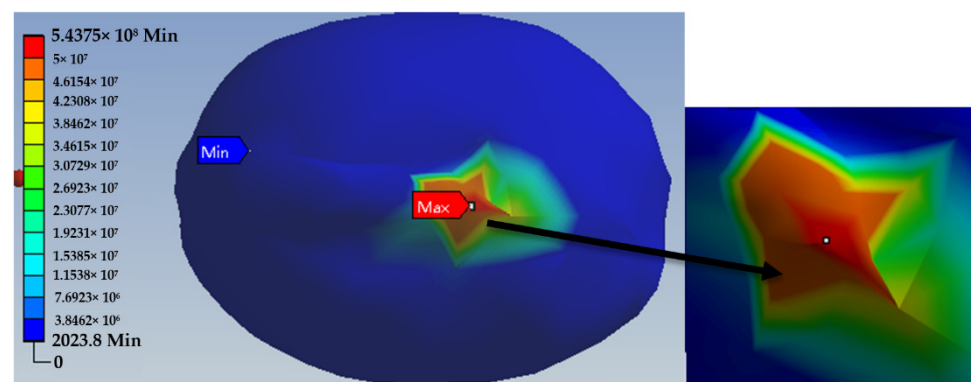


Figure 12. Stress cloud map of the walnut under unidirectional load.

5. Walnut Shell Breaking Experiments under Unidirectional Load

According to the requirements of walnut shell breaking under unidirectional load, this study designed a mechanical claw shell-breaking test bench (Figure 13) to carry out the walnut shell breaking tests under unidirectional load.

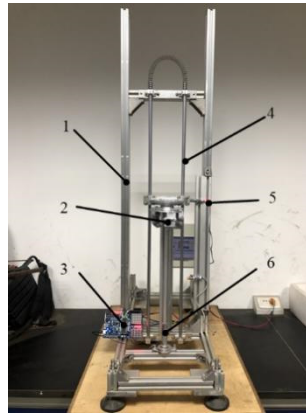


Figure 13. Mechanical claw shell breaking test bench. (1) Frame; (2) Three-fingered mechanical claws; (3) Microcontroller; (4) Sliding rail; (5) Proximity switch; (6) Impact table.

5.1. Test Procedure

On the test bench, a large walnut sample was grabbed by a three-fingered mechanical claw with the walnut ridge parallel to the impact table and the midpoint of the walnut shell surface touching the impact table when impacting, and then the mechanical claw was lifted to different heights to enable it to fall freely along the sliding rail until the walnut fell on the impact table to implement unidirectional load.

According to the momentum theorem, the force the walnut undertook was calculated by Equation (16).

$$F \cdot t = mv_2 - mv_1 \quad (16)$$

where F is the force, which is unknown; t is the action time, which was set as 0.01 s; m is the mass; v_1 is the initial velocity; v_2 is the final velocity; both v_1 and v_2 are vectors.

The overall mass of the mechanical claws was 1.6 kg. In the experiment, walnuts and the impact table collided with almost no rebound, and thus $v_2 = 0$, and v_1 was measured as follows. Two proximity switches were installed on the test bench framework, the spacing of which was the calibration value X_0 . The first proximity switch position was set as the starting position, and the second was set as the termination position. After the mechanical claw was placed at the starting position, the microcontroller was turned on. Then the mechanical claw was released to fall freely along the sliding rail. At this time, the timing program of the microcontroller was triggered to start timing. When the mechanical claw reached the termination position, the proximity switch was triggered again. Subsequently, the microcontroller stopped timing immediately after receiving the signal from the proximity switch, and t_0 (the time when the mechanical claw moved from the initial position to the termination position) was output and displayed. Then, according to the displacement formula $x = 1/2 at^2$, the acceleration (a) of the mechanical claw to fall freely along the sliding rail was calculated as 9.8 m/s². Finally, the base of the impact table in the test bench was taken as the zero point, and X_0 (the spacing between the two proximity switches) was calibrated with 10 cm as the unit distance along the sliding rail. From different heights (h), the mechanical claw was released to fall freely along the sliding rail until the walnuts collided with the impact table and the shell broke. The velocity v during the impact was calculated by the formula $v^2 = 2ax$. a and x (namely, h) were substituted into the formula, and the v value (the initial velocity v_1 in Equation (16)) was obtained.

5.2. Test Results

The shell load force was calculated as follows. Based on multiple tests, the critical height for walnut shell breaking (h) was determined as 20 cm. When the height was above 20 cm, the walnut would be seriously broken. When the height was below 20 cm, the walnut failed to break. According to $v^2 = 2ax$, the initial velocity is $v_1 = 1.98$ m/s. In addition, when $t = 0.01$ s, $m = 1.6$ kg, $v_1 = 1.98$ m/s were substituted into the Equation (16), the load force F was calculated as 316.8 N in the process of collision, which was consistent with the results obtained by the equation in Section 2.3.

After the shell-breaking tests, the walnut cracks were analyzed (Figure 14). The crack expansion direction was consistent with our hypothesis of fracture along the longitudinal texture. The shell and kernel were separated from the walnut kernel intact; therefore, the shell-breaking effect was desirable.



Figure 14. Walnut shell crack and complete kernel after shell-kernel separation.

6. Discussion and Conclusions

In this study, the spherical thin-shell model was established for walnut shell breaking tests, and the model fitting degree was tested by the elastic mechanical calculation based on the spherical thin-shell theory. The model deviation was found to be within 5%, indicating a good fitting degree of the model. Based on theoretical analysis of this model and walnut shell breaking experiments, the following conclusions were drawn:

- (1) The walnut shell was divided into the concentrated force region and peripheral force region. In the peripheral force domain, the internal forces of the shell surface in all directions were calculated to be equal based on the momentless theory. In the concentrated force region, the finite element analysis method was used to intuitively exhibit the gradient distribution of the internal force on the shell from inside to outside. Based on these results, we suggested that the unidirectional force during shell breaking should be loaded on the middle of the walnut shell surface so as to make the shell surface force load uniform, thus improving the shell breaking effect and efficiency.
- (2) Walnut cracks included type I and type II cracks. According to the maximum stress yield criterion, crack initiation occurred at the position where the load was applied, and the crack expansion direction was determined according to the fracture criterion and the stress intensity factor. Finally, the crack expansion rate could be used to determine the walnut shell breaking position and force loading time so as to obtain the complete kernel and improve the shell-kernel separation rate.
- (3) The actually measured walnut shell breaking force under unidirectional load was in line with the theoretical value, and the observed crack extension direction was consistent with our hypothesis of fracture along the longitudinal texture. These results jointly verified the reliability of the theoretical model proposed in this study. Our results can provide a theoretical basis for the development and structural optimization of shell-breaking machinery.

Author Contributions: Conceptualization, X.B. and J.M.; methodology, X.B. and J.M.; software, P.D.; validation, B.C.; resources, X.B.; data curation, P.D. and Y.L.; writing—original draft preparation, B.C.; writing—review and editing, X.B. and J.M.; project administration, X.B. All authors have read and agreed to the published version of the manuscript.

Funding: This research was funded by the Nature Science Foundation of Hubei Province, China (No. 2021CFB 471), and the Nation Key Research and Development Program of China (No. 2018YFD0700804), and the National Natural Science Foundation of China (No. 51605181).

Institutional Review Board Statement: Not applicable.

Informed Consent Statement: Not applicable.

Data Availability Statement: Not applicable.

Conflicts of Interest: The authors declare no conflict of interest.

References

1. Song, Y.; Wang, X.H.; Zhang, R.; Liu, C.H.; Yu, S.Q.; Gao, S.; Zhang, R.L. Comparison of Quality Differences Among Varieties of Walnut from Xinjiang. *J. Chin. Cereals Oils Assoc.* **2019**, *34*, 91–97.
2. Lu, J.; Zhao, A.Q.; Cheng, C. Nutritional composition and physiological activity of walnut and its development and utilization. *Food Mach.* **2014**, *30*, 238–242.
3. Sütyemez, M.; Bükücü, Ş.B.; Özcan, A. ‘Helete Güneşi’: A New Walnut Cultivar with Late Leafing, Early Harvest Date, and Superior Nut Traits. *Agriculture* **2021**, *11*, 991. [[CrossRef](#)]
4. Aleksandra, V.C.; Marie-Christine, R.; Jacqueline, V.; Sara, K.; Arijana, M.; Draženka, K.; Estelle, B. Valorisation of walnut shell and pea pod as novel sources for the production of xylooligosaccharides. *Carbohydr. Polym.* **2021**, *263*, 117932.
5. Liu, M.Z.; Li, C.H.; Cao, C.M. Research progress of key technology and device for size-grading shell-breaking and shell-kernel separation of walnut. *Trans. Chin. Soc. Agric. Eng.* **2020**, *36*, 294–310.
6. Wang, J.; Liu, M.; Wu, H.; Peng, J.; Peng, B.; Yang, Y.; Cao, M.; Wei, H.; Xie, H. Design and Key Parameter Optimization of Conic Roller Shelling Device Based on Walnut Moisture-Regulating Treatments. *Agriculture* **2022**, *12*, 561. [[CrossRef](#)]
7. Khir, R.; Pan, Z.; Atungulu, G.G.; Thompson, J.F.; Shao, D. Size and moisture distribution characteristics of walnut and their components. *Food Bioprocess Technol* **2013**, *6*, 771–782. [[CrossRef](#)]
8. Froogh, S.; Mohammadali, H.D. Mechanical behavior of walnut under cracking conditions. *J. Appl. Sci.* **2008**, *8*, 886–890.
9. Koçturk, B.O.; Gurhan, R. Determination of mechanical properties of various walnut according to different moisture levels. *J. Agric. Sci.* **2007**, *13*, 69–74.
10. Wu, Z.Y. Mechanical analysis of walnut shelling. *J. Nanjing Agric. Univ.* **1995**, *18*, 116–123.
11. Tu, C.; Yang, W.; Yin, Q.J. Optimization of technical parameters of breaking macadamia nut shell and finite element analysis of compression characteristics. *Trans. Chin. Soc. Agric. Eng.* **2015**, *31*, 272–277.
12. Yan, R.; Gao, J.; Zheng, J.H. Analysis of mechanical properties of walnut shell breaking based on workbench. *Agric. Mech. Res.* **2014**, *36*, 38–41.
13. Ojolo, S.J.; Damisa, O.; Orisaleye, J.I. Design and development of cashew nut shelling machine. *J. Engineering. Des. Technol.* **2010**, *8*, 146–157. [[CrossRef](#)]
14. Li, Z.X.; Liu, K.; Yang, L.L. Design and experiment of cone basket walnut shell breaking device. *J. Agric. Mach.* **2012**, *43*, 146–152.
15. Liu, M.Z.; Li, C.H.; Zhang, Y.B. Shell Crushing Mechanism Analysis and Performance Test of Flexible-belt Shearing Extrusion for Walnut. *Trans. Chin. Soc. Agric. Mach.* **2016**, *47*, 266–273.
16. Ding, R.; Cao, C.M.; Zhan, C. Design and experiment of bionic-impact type pecan shell breaker. *Trans. Chin. Soc. Agric. Eng.* **2017**, *33*, 257–264.
17. Xu, B.H.; Wang, Y.X.; Zhao, Y.H. Advances in the study of the toughness of wood-stripped fractures. *Mech. Pract.* **2016**, *38*, 493–500.
18. Norman, E.D.; Jiang, S.Y.; Zhang, Y.Q. *Mechanical Behavior of Engineering Materials*; China Machine Press: Beijing, China, 2015.
19. Law, B.; Gong, J.H. *Fracture Mechanics of Brittle Solids*; Higher Education Press: Beijing, China, 2010.